Colloids and Surfaces A: Physicochemical and Engineering Aspects 655 (2022) 130320

Contents lists available at ScienceDirect

Colloids and Surfaces A: Physicochemical and Engineering Aspects

journal homepage: www.elsevier.com/locate/colsurfa

Occurrence characteristics and influential factors of movable oil in nano-pores by molecular dynamics simulation

Yongcheng Luo [a,b,c], Hanmin Xiao [b,c,*], Xiangui Liu [b,c], Taiyi Zheng [d,**]

[a] College of Engineering Science, University of Chinese Academy of Sciences, Beijing 100049, China
[b] Institute of Porous Flow and Fluid Mechanics, University of Chinese Academy of Sciences, Langfang 065007, China
[c] Research Institute of Petroleum Exploration & Development, Beijing 100083, China
[d] Institute of Mechanics, Chinese Academy of Science, Beijing 100190, China

HIGHLIGHTS

- Distribution profile of adsorbed and free crude oil in various nanoslits.
- The self-diffusion coefficient and potential energy of crude oil at different positions.
- Temperature has a great influence on the occurrence state of crude oil.
- Effects of different proportions of CO_2 on the occurrence state of crude oil in nanoslits.

GRAPHICAL ABSTRACT

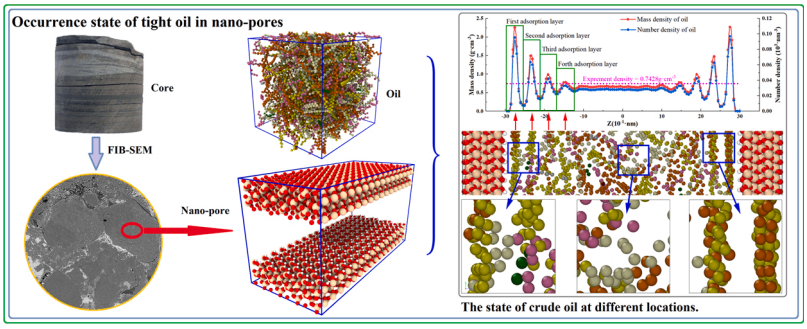

ARTICLE INFO

Keywords:
Adsorption
Potential energy
Self-diffusion coefficient
Molecular dynamics
Nano-pores

ABSTRACT

CO_2-enhanced oil recovery (CO_2-EOR) technology has shown great application potential in the development of tight reservoirs. Since the proportion of nano-pores in tight oil reservoirs exceeds 77%, it is necessary to further study the occurrence state of crude oil in nano-pores. In this paper, the molecular dynamics simulation was applied to study the adsorption and diffusion behaviors of multi-component crude oil in quartz (hydrophilic) nano-pores. Besides, the density discretization method was used to investigate the occurrence characteristics of crude oil, the proportion of movable fluid in nano-pores, and the effects of CO_2 and polar molecules (C_3H_6O) on the adsorption characteristics of crude oil. The simulation results showed that the adsorption state of crude oil in the quartz nano-pores was in the form of 4 adsorption layers with a thickness of 0.45 nm each. In nano-pores, the oil molecules with longer molecular chains were more likely to aggregate and adsorb on the quartz surface. Among them, polar oil molecules have the strongest adsorption capacity on the quartz surface. Moreover, the crude oil potential energy and the self-diffusion coefficient gradually increased from the vicinity of the quartz wall and tended to be stable in the free layer. Meanwhile, the content of movable crude oil gradually augmented with the increasement of nanometer pore width and temperature. Furthermore, the pressure had little effect on the density distribution of crude oil in the pores. In contrast, the temperature had a more significant effect on the density distribution of the adsorption layer. At last, due to the more substantial adsorption capacity of CO_2 on the

* Corresponding author at: Institute of Porous Flow and Fluid Mechanics, University of Chinese Academy of Sciences, Langfang 065007, China.
** Corresponding author.
E-mail addresses: xiaohm69@petrochina.com.cn (H. Xiao), zhengtaiyi@imech.ac.cn (T. Zheng).

https://doi.org/10.1016/j.colsurfa.2022.130320
Received 12 August 2022; Received in revised form 30 September 2022; Accepted 6 October 2022
Available online 10 October 2022

rock surface, the crude oil adsorbed initially on the rock surface would be stripped off by CO_2, converting from irreducible oil to moveable oil.

1. Introduction

With the continuous growth of global energy demand in recent years, unconventional resources such as tight oil have become an indispensable share of oil and gas production [1–3]. However, for the tight oil reservoir, the extremely low porosity-permeability [4,5], the heterogeneous and complex micro-structure [6,7], and other characteristics can compound the difficulty of oil production.

With minor porosity and permeability, tight oil reservoirs have pores mainly in microns and Nanos, where the nano-pores account for more than 77% of the total pore content [8–10]. Nano-pores dramatically increase the proportion of adsorbed oil in the tight reservoir, making the occurrence state of tight oil complex and diverse. Wang et al. [11] studied the tight oil microscopic state of Chang7 by nuclear magnetic resonance (NMR) and micrometer-nanometer CT Scanning technology. Their results showed that the oil existence states in tight reservoirs were divided into six types (thin film form, cluster form, throat form, emulsion form, particle form, and isolation form). The emulsion and thin film forms were the leading existence states (70%). Gong et al. [12] used Energy Dispersive Spectroscopy (EDS) and Environmental Scanning Electron Microscope (ESEM) to detect tight oil occurrences in micro- and nano-pores, where the occurrences primarily existed in the form of oil film and then in the form of oil drop. Li et al. [8] pointed out that the adsorbed tight oil was primarily distributed on the surface of mineral particles, mica fragments, fractures, throats, and dissolved pores, in the shape of films with variable thicknesses and long strips. The proportion of adsorbed tight oil in the total crude oil was the highest at 67.52%, the lowest at 39.05%, and the average at 49.86%. Applying the microfluidic chip and micro-CT scanning tests, Liu et al. [13] found that the oil film thickness in microscale pores was negatively correlated with temperature and positively correlated with pore size. Moreover, the proportion of immobile and movable states was also strongly linked with the fluid compositions.

In addition, the injection medium is likewise a key factor affecting the tight oil occurrence state. Cao et al. [14] analyzed the effect of CO_2 adsorption on oil displacement in tight reservoirs, concluding that the adsorption capacity of reservoir minerals for CO_2 was more significant than that for hydrocarbons. Due to the large number of nanoscale pores in tight reservoirs, it is necessary to further analyze the adsorption process of crude oil after CO_2 injection to understand the mechanism of CO_2-enhanced oil recovery.

Experimentally, a series of experimental techniques, such as quantitative grain fluorescence (QGF), nano-CT, environmental scanning electron microscope combined with energy-dispersive spectrometry (ESEM-EDS), NMR, and core displacement (Physical simulation) have been used to study the tight oil movability [15]. The current study of the movable fluid saturation in nano-pores after CO_2 injection is unclear. The movable fluid saturation can reflect the occurrence state of the fluid in the pores [16,17]. Movable fluid saturation has always been considered one of the critical parameters for reservoir quality evaluation and oil and gas reserves calculation. It is of great value to the characteristics of fluid occurrence in pores [5,18]. However, these experimental methods are still insufficient to reveal the crude oil distribution state and the movable oil proportion in nano-pores.

Numerically, molecular dynamics (MD) simulation can be used to analyze the oil occurrence state and oil adsorption behavior. Using MD simulations, Hekmatifar et al. [19] used MD methods to estimate the effects of various physical parameters such as temperature, pressure, and desorption of TiO2 nanoparticles on asphaltenes from iron surfaces. Yang et al. [20] revealed the adsorption properties of surfactants at the oil-water interface. Wu et al. [21] used MD simulations to study the adsorption behavior of methane on kaolinite. The adsorption energy and isotherm obtained by MD simulation are similar to those brought by isothermal titration calorimetry (ITC) and batch experiments, which verifies the reliability of MD simulation. Yang et al. [22] quantitatively studied the adsorption behavior of shale oil in kerogen fractures. Using MD simulations, Hong et al. [23] investigated the competitive adsorption of asphaltene and n-heptane on quartz surfaces. They found that the adsorption capacity of asphaltene on quartz surfaces is much stronger than that of n-heptane. Sui et al. [24] studied the adsorption of n-octane in nanoscale slit-pores. However, the liquid systems chosen by most researchers are single-component systems, which cannot sufficiently represent crude oil.

Although scholars have begun to study the occurrence state of crude oil in tight reservoirs, there are few studies on the distribution characteristics of multi-component crude oil in nano-pores. In particular, the potential energy distribution of crude oil in nano-pores and the effect of CO_2 on the occurrence state of crude oil have not been well studied. This paper used the MD simulation method to establish a series of MD models. In this way, the occurrence state of crude oil in the nano-pore and the influence of CO_2 on the occurrence state of crude oil were studied. The existence and distribution characteristics of crude oil's adsorbed and free states in the nano-pore were clarified. Moreover, the models explored the potential energy distribution and crude oil self-diffusion coefficient in nano-pores. It also analyzed the effect of dissolved CO_2 on the oil occurrence state in nano-pores.

2. Molecular models and simulation methods

2.1. Models

The pore structure of the Chang-7 reservoir matrix is complex. Through X-ray diffraction (XRD), mercury porosimetry, helium pycnometry, low-pressure N_2 adsorption experiments, and the fractal method, Shan et al. [25] found that the pore size of the Chang-7 reservoir matrix was mainly from nanometer to micrometer, where the pore diameter was ranging from 1.5 to 5 nm. Bu et al. [26] believed that most pores in tight reservoirs were cylindrical or slit-shaped. Wang et al. [27] used circular tubes and slits to characterize the complex pores to facilitate calculations. Using MD simulation, Song et al. [28] compared the fluid density distribution in cylindrical and slit-shaped pores of the same size and found no noticeable difference in fluid density distribution in the previous pore structures.

Therefore, in this paper, slit-shaped pores were applied to study the occurrence state of tight oil. As sedimentary rocks were hydroxylated, they were initially water saturated. The hydrophilic silica surface was obtained by cutting the bulk crystal of α-quartz along the [0 0 1] direction and then artificially adding H atoms to the new silica surface to represent the natural geological conditions [29,30] (Fig. 1(a)).

For the crude oil model, a quaternary system (C_6, C_{10}, C_{19}, C_{30}) has been successfully used to estimate the minimum miscible pressure, crude oil swelling properties, and diffusion properties in the CO_2-crude oil system. [31,32]. In addition, it can be considered to add light oil components, C_1-C_4, to the multi pseudo component system to obtain better simulation results. Hence, in this paper, an eight components system (C_1-C_4, C_6, C_{10}, C_{19}, C_{30}) was adopted for the molecular simulation according to the component analysis of Chang-7 crude oil (Fig. 1 (b-c)).

2.2. Force field models

The choice of force field parameters is directly related to the

accuracy of MD simulation. Appropriate and reliable potential energy parameters can more accurately simulate the macroscopic properties of the system.

In this paper, we use different force field potential energy parameters for different molecular groups (the EPM2 force field [33], the TraPPE-UA force field [34,35], and the NERD force field [36] in turn acted on CO_2 and C_3H_6O, CH_4 and all other alkanes [32]. The CLAYFF force field [37] adopted quartz substrates). The pairwise additive Lennard-Jones (LJ) 12–6 potentials and the coulombic interactions described the nonbonded interactions between atoms.

The standard 12/6 Lennard-Jones potential, given by

$$E = 4\epsilon\left[\left(\frac{\sigma}{r}\right)^{12} - \left(\frac{\sigma}{r}\right)^{6}\right] \tag{1}$$

The Coulombic pairwise interaction, given by

$$E = \frac{Cq_iq_j}{\epsilon r} \tag{2}$$

Where C is an energy-conversion constant, q_i and q_j are the charges on the 2 atoms, ϵ is the dielectric constant, σ represents the distance at which interaction energy of two particles is minimal, and r is the distance between 2 particles.

Unlike-atom interactions were calculated using the modified Lorentz-Berthelot combining rules [32,38].

$$\sigma_{ij} = \frac{\sigma_{ii} + \sigma_{jj}}{2} \tag{3}$$

$$\epsilon_{ij} = a\sqrt{\epsilon_{ii}\epsilon_{jj}} \tag{4}$$

Here, a= 0.9 was adopted for CO_2-alkanes interactions, while a= 1 for all other interactions.

2.3. Molecular simulation details

The molecular model with constant volume-temperature (NVT ensemble) was proceeded in the CO_2-oil system, where the temperature and pressure were respectively controlled by the Nose-Hoover thermostat and Berendsen method [39].

In the pore system containing CO_2-Oil, NVT ensemble was used for relaxation calculations. The temperature was controlled at 380.15 K by using a Nose-Hoover thermostat. Since the system was a multi-component, the pressure of the CO_2-crude oil system was controlled by the He nanoplates on both sides (Fig. 3). The pressure P was applied simultaneously on the He nanoplates in the left and right so that the pressure of the fluid in the pore was P.

For systems containing CO_2, the particle-particle particle-mesh (PPPM) method was used to calculate long-range electrostatic interactions with an accuracy of 10^{-5}. The cutoff radius was set to 12.0 Å, and the time step was set to 1 fs. All simulations considered periodic boundary conditions.

In the pore fluid model, the entire pore and CO_2-Oil system were firstly equilibrated in NVT simulation by applying pressure P within 1 ns. Then fix the left and right He nanoplates and perform NVT equilibrium simulation within 1 ns. Finally, perform NVT simulation within 1 ns to collect data. The data was collected within the 5 nm broad region of the pore laterally (in the red box in Fig. 1(d)). All molecular simulations were performed using the Lammps software package, and images were rendered using the Ovito software.

3. Results and discussion

3.1. Density distribution and distribution of different components

To study the occurrence state of crude oil in nano-pores, the density distribution of various components in crude oil from the inner wall of pores to the middle of the pores was investigated in a 6-nanometer pore under the conditions of 380.15 K and 10.0 MPa.

To count the density distribution perpendicular to the quartz surface, it was assumed that the density in the interval of ΔZ= 0.05 nm was continuous during the simulation. Fig. 2(a) shows crude oil's mass density distribution and number density distribution in the 5.92 nm pore. As shown in Fig. 2(a), the distribution curves of mass density and number density were generally consistent. Moreover, the two density curves of crude oil were roughly symmetrical on the positive and

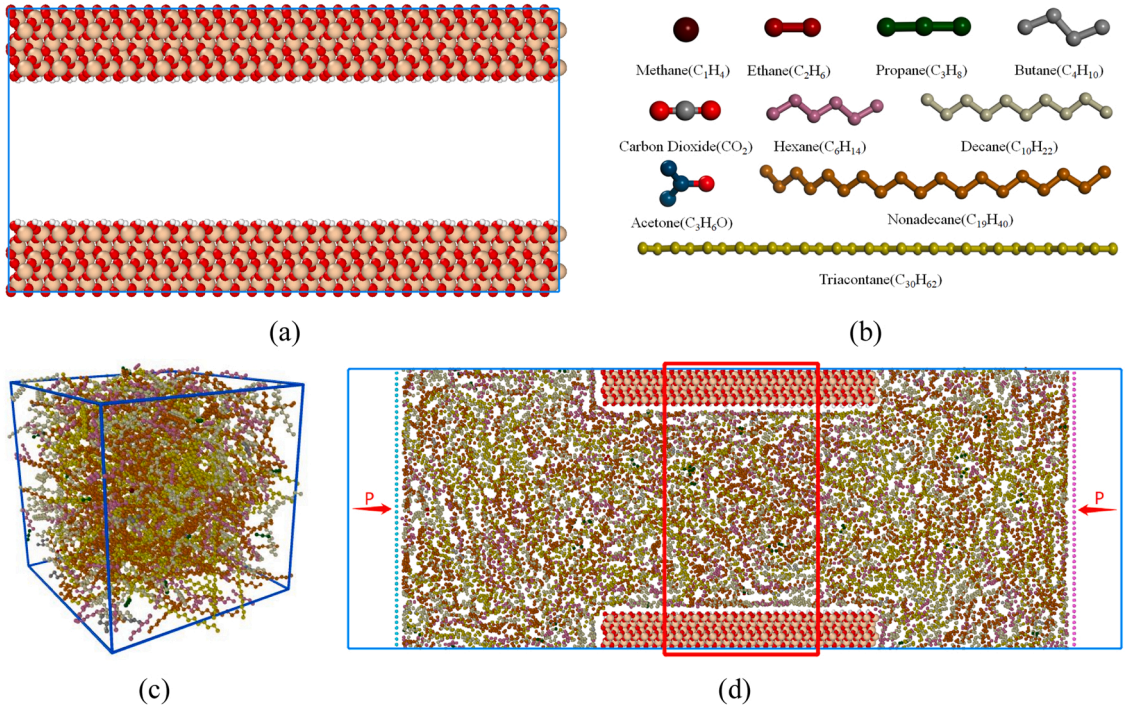

Fig. 1. Schematic diagram of MD model: (a) a quartz pore, (b) CO_2 and hydrocarbon molecules, (c) molecule of crude oil, and (d) combined model.

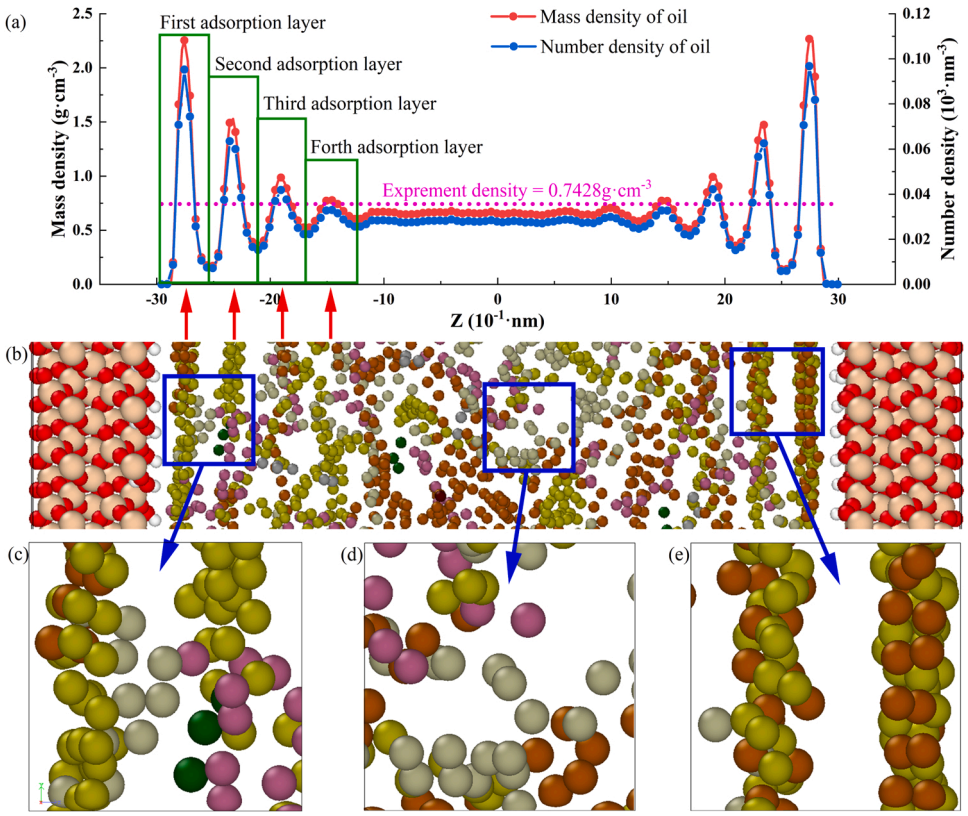

Fig. 2. Distribution characteristics of crude oil at a temperature of 380.15 K and a pressure of 10 MPa: (a) Mass density and number density distribution of crude oil, (b) Distribution state of crude oil in 5.92 nm pores, (c) Occurrence state of crude oil on the left wall, (d) Occurrence state of crude oil in the middle, (e) Occurrence state of crude oil on the right wall.

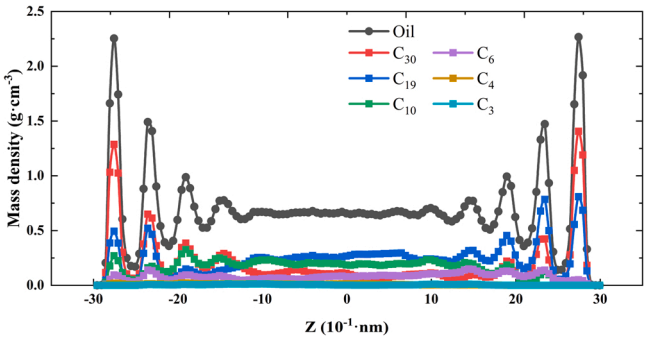

Fig. 3. Mass density distribution of different components in crude oil in 5.92 nm pore at the temperature of 380.15 K and pressure of 10 MPa.

negative sides of the Z axis. To conveniently analyze the characteristics of the crude oil occurrence, only the left half of the z-axis of the mass density in the pore was expressed below.

Fig. 2(a) showed that the average bulk density of crude oil calculated by MD from z = −1.0 nm to Z = 1.0 nm was 0.6690 g·cm^{-3}, while the density measured by the experiment was 0.7428 g·cm^{-3}. This was because C30 was applied in the MD model to uniformly represent the C30 + molecules of the actual crude oil components, resulting in a lower density calculated by the model than that measured by the experiment. Moreover, the mass density of crude oil fluctuated near the quartz surface (z = ± 3 nm), and the fluctuation range increased as it got closer to the quartz surface. The peak density closest to the quartz surface was 2.2541 g·cm^{-3}, which was 3.35 times the bulk density. This phenomenon showed that crude oil molecules were adsorbed on the quartz surface, with multiple adsorption layers. As the distance from the quartz surface increased, the interaction between solid and liquid decreased, and the peak value of the adsorption layer gradually reduced. In particular, although the peak value of each adsorption layer was different, the thickness of each adsorption layer was basically the same, about 0.45 nm.

From the molecular perspective, Fig. 2(b-e) visually showed that the molecules near the wall were arranged orderly, and the arrangement direction of crude oil molecules was mainly parallel to the quartz surface [27,40]. As the distance from the quartz surface increased, the arrangement direction of the crude oil gradually became disordered.

Considering the complex composition of crude oil, the distribution state of crude oil in pores cannot be genuinely reflected with a single oil component. In this study, the density distributions of different components of crude oil (C_3, C_4, C_6, C_{10}, C_{19}, and C_{30}) in 5.92 nm pores were statistically analyzed in Fig. 3. To explore the adsorption capacity of different components in the nano-pore, the ratio of the first adsorption layer to its bulk density was compared since the number of molecules and molecular masses of various components were different. As shown in Fig. 3, the ratio of the peak value of C30 to its bulk density was the highest in the first adsorption layer. As the number of carbon atoms decreased, the above ratio decreased accordingly. This showed that in nano-pores, molecules with longer molecular chains in crude oil were more likely to aggregate and adsorb on the quartz surface, making crude oil more challenging to be exploited.

3.2. Adsorption energy and self-diffusion coefficient

The adsorption energy is a momentous parameter for the liquid-solid interface interaction. It is known that the lower the adsorption energy, the stronger the adsorption capacity [41]. The magnitudes of interaction between crude oil and quartz surface can be characterized by adsorption energy. The formula for calculating the adsorption energy is as follows

[41,42]:

$$\Delta E_{ads} = E_{total} - E_{oil} - E_{quartz}$$

Where ΔE_{ads} is the adsorption energy (kcal·mol^{-1}), E_{total} represent the total potential energy of phases oil and quartz in contact at equilibrium (kcal·mol^{-1}), E_{oil} and E_{quartz} are the potential energy of separated oil and quartz in vacuum at equilibrium (kcal·mol^{-1}), respectively.

Adhesion work can quantitatively characterize the interface's bonding strength, which also has been widely used to describe the interaction intensity between two substances [43]. The formula of adhesion work is [44,45].

$$W_{ads} = \frac{\Delta E_{ads}}{S}$$

Where S is the interfacial contact area between oil and quartz.

In addition, the migration mechanism of crude oil on the quartz surface can be reflected by the self-diffusion coefficient [24]. To obtain the self-diffusion coefficient, the quartz pores with a thickness of 0.45 nm were divided into 7 plates along the z-axis direction in the numerical model, where plates 1–4 were adsorbed crude oil, and plates 5–7 were free crude oil. Then, each plate's self-diffusivity was calculated using the relation of mean square displacement (MSD) versus time slope. The self-diffusion coefficient of crude oil in different blocks can be obtained by the following formula [46,47]:

$$MSD(\Delta t) = \frac{1}{\tau - \Delta t}\int_0^{\tau-\Delta t}[r(t-\Delta t) - r(t)]^2 dt = \langle [r(t-\Delta t) - r(t)]^2 \rangle \quad (5)$$

$$D_{self} = \lim_{\Delta t \to \infty} \frac{dMSD(\Delta t)}{6d\Delta t} \quad (6)$$

Where τ was the total simulation time, s; MSD was the mean square displacement, m^2; $r(t)$, $r(t-\Delta t)$ were respectively the positions at t time and $t-\Delta t$ time, s.

In order to explain the adsorption of crude oil on the quartz surface, an MD model of crude oil in the quartz pore was established to calculate the crude oil potential energy in different plates (Fig. 4(a)). The simulation results showed that the crude oil potential energy in the first adsorption layer was the lowest (−4.86 kcal·mol^{-1}). The atoms in the first liquid layer were preferentially located in the potential energy valley, which was the reason for the order of the liquid structure at the solid-liquid interface [48]. With the increase of the adsorption layer, the crude oil potential energy aggrandized gradually and became positive after the second layer. This was mainly due to weakening the non-bonded pairwise interactions between the liquid and solid molecules away from the wall [49,50]. As is well known, the lower the potential energy, the more stable the state of matter. Therefore, the adsorption of crude oil on the quartz surface reduced its potential energy, resulting in the crude oil near the quartz surface becoming stable and challenging to move. For liquid-solid interfaces, the contact area can be regarded as the cross-sectional area of the model. Based on the potential energy difference before and after crude oil adsorption, the work of crude oil adsorption force in the 5.92 nm quartz pore was calculated to be − 8.02 kcal·mol^{-1}·nm^{-2}.

To explore the migration mechanism of crude oil in different adsorption layers, the self-diffusion coefficients of crude oil in different plates were calculated (Fig. 4(b)). It can be seen from the figure that the self-diffusion coefficient decreased in the vicinity of the quartz wall, and the lowest value was 1.72 × 10^{-8} m^2·s^{-1} in the first adsorption layer. Moreover, the free layer's self-diffusion coefficient tended to be stable, about 6.0 × 10^{-8} m^2·s^{-1}. These results indicated that the movement of crude oil molecules near the quartz surface was more easily inhibited than in the central pore region.

3.3. Tight oil occurrence state and movability

In the pore-fracture system of tight reservoirs, crude oil was attached to the mineral particles' surface or adsorbed by organic matter, existing in adsorbed or free states [24,27,44]. According to the statistics, the proportion of adsorbed tight oil to the total tight oil amount was the highest at 67.52%, the lowest at 39.05%, and the average at 49.86% [51]. Meanwhile, according to NMR analysis, Wang et al. [52] believed that the relative content of adsorbed tight oil in the Chang 7 reservoir accounted for between 50% and 68%. At present, there are insufficient studies on the occurrence state and movability of crude oil in nano-pores in tight reservoirs. Hence, this paper focused on the oil occurrence characteristics in fine pores in the tight reservoir.

Adsorbed crude oil mass was indirectly estimated by the thickness of the adsorbent layer. Christenson et al. [53] measured the thickness of each adsorption layer of n-alkanes on the mica surface to be 0.40–0.50 nm. Wang et al. [27] showed that the monolayer adsorption thickness of n-Alkanes on quartz surface was 0.48 nm. As shown in Fig. 5, the thickness of the first adsorption layer on the quartz surface was 0.45 nm, while the total thickness was 1.8 nm. Fig. 5(b) revealed the discretized crude oil density for each adsorption layer inside the pore, where the density of the first adsorption layer was 0.7852 g·cm^{-3}, and the fourth was 0.6737 g·cm^{-3}. The formula for calculating the crude oil mass in the pore is as follows:

$$m_{ab-i} = V_i \rho_i$$

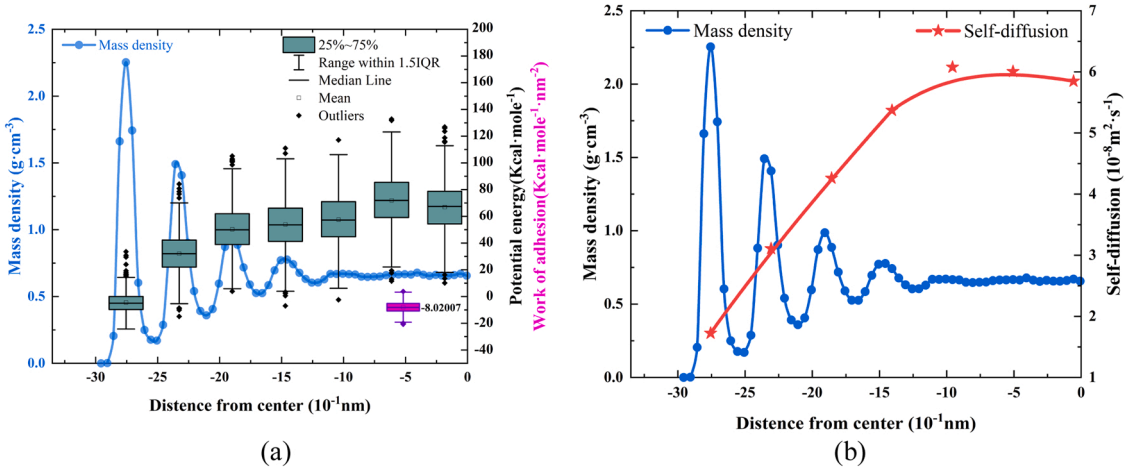

Fig. 4. Characteristics of crude oil at different positions within a 5.92 nm pore at the temperature of 380.15 K and pressure of 10 MPa: (a) Potential energy and adsorption energy of crude oil at different positions, (b) Diffusion coefficient of crude oil at different positions.

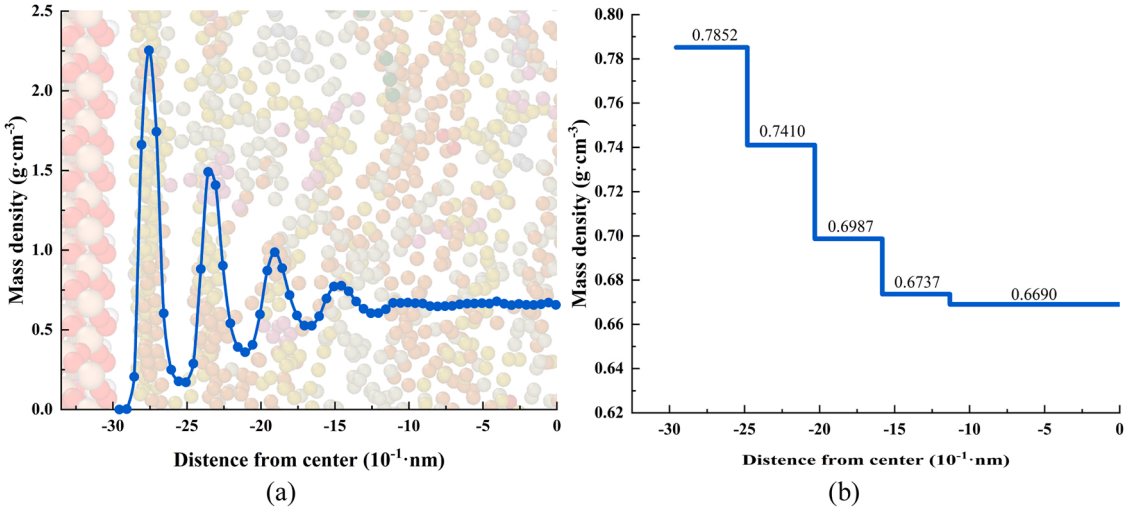

Fig. 5. Mass density distribution of crude oil in a 5.92 nm pore at a temperature of 380.15 K and a pressure of 10 MPa: (a) Mass density distribution of crude oil, (b) Discretization of crude oil mass density distribution.

$$m_{total} = V_{bv}\rho_{bd} + \sum_i^N m_{ab-i}$$

Where, m_{ab-i} is adsorbed mass of layer ith; V_i is adsorbed volume of layer ith; ρ_i is adsorbed density of layer ith; V_{bv} is the bulk volume; V_{bd} is the bulk density.

The ratio of the mass of adsorbed crude oil to the total mass of crude oil can be calculated by the following formula:

$$P_{rop} = \frac{\sum_i^N m_{ab-i}}{m_{total}}$$

Therefore, it can be calculated that the amount of crude oil adsorbed on the quartz surface in the 5.92 nm pore was 62.80%. Since adsorbed crude oil was difficult to recover, it was considered that free crude oil can be recovered. Therefore, the recovery factor was 37.20%.

$$R = 1 - P_{rop} = 37.20\%$$

3.4. Pore throat size on the crude oil occurrence state

The size of nano-pores greatly influences the crude oil occurrence state. Then, a series of molecular models were established to observe the oil distribution state in nano-pores with different scales under the conditions of 10 MPa and 380.15 K. Fig. 6 showed the oil density distribution in pores with widths ranging from 1.92 nm to 11.92 nm. According to the description in the previous section, the thickness of each adsorption layer was 0.45 nm. It can be seen from the figure that all the pores with a width less than 1.92 nm were filled with adsorbed oil. As the pore width increased, the number of adsorption layers increased accordingly until reaching the fourth layer. Thus, the number of adsorption layers was not directly related to the width of the pore, which only depended on the adsorption capacity of the rock wall to alkane molecules. Moreover, as the width of the nano-pore increased, the peak value of the first adsorption layer gradually augmented with a smaller amplitude. Fig. 7 expressed that the proportion of movable crude oil was 0% in the 1.92 nm pore, while 7.34% in the 3.92 nm pore. This

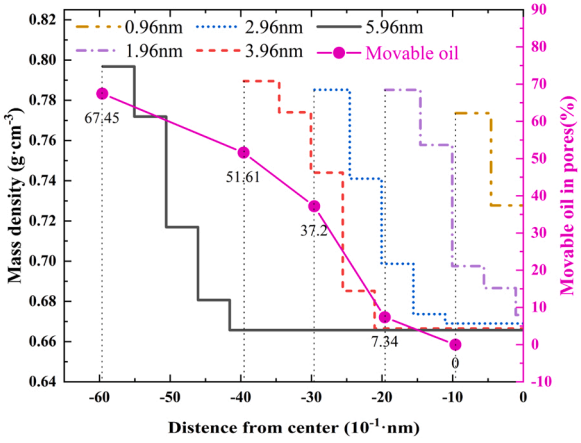

Fig. 7. Mass density discretization distribution and movable oil proportion of crude oil in nano-pores of different sizes at a temperature of 380.15 K and a pressure of 10 MPa.

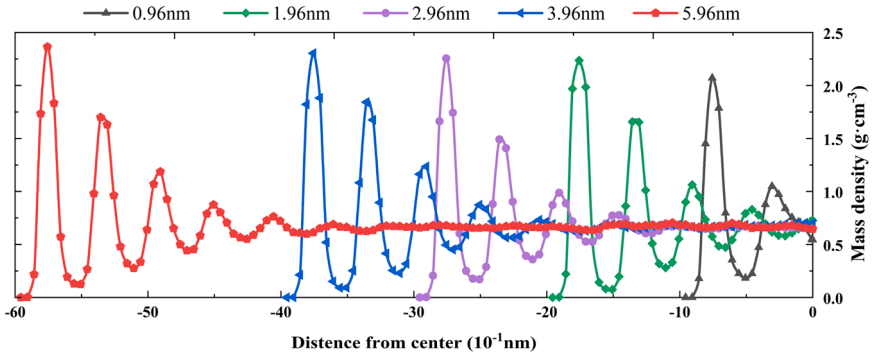

Fig. 6. Mass density distribution of crude oil in nano-pores of different sizes at a temperature of 380.15 K and a pressure of 10 MPa.

proportion was positively correlated with the pore width.

3.5. Pressure and temperature on the crude oil occurrence state

Pressure and temperature are key parameters for studying the crude oil occurrence state in nano-pores. In this paper, the density distribution of crude oil at three pressures and three temperatures was compared and analyzed. From Fig. 8(a), the pressure had little effect on the oil density distribution in nano-pores. Explicitly, the oil density distribution was almost accordant in the first and the second adsorption layer under the three pressure conditions. While in the third or fourth layer to the bulk region, an increase in pressure can lead to a slight increase in density. This was because capillary condensation occurred under in situ conditions, and the adsorption capacity remained constant with increasing pressure [27,54].

From Fig. 8(b), the temperature obviously affected the oil density distribution of the adsorbed layer. The higher the temperature, the lower the oil density. Since the average kinetic energy was proportional to the temperature, at higher temperatures, the greater the kinetic energy, the easier the separation of crude oil molecules from the solid wall. As a result, adsorption was inhibited in the near-wall region, providing the possibility for thermal recovery.

Fig. 9 showed that the movable crude oil could increase from 36.72% to 37.26% when the temperature changed from 360.15 K to 400.15 K. However, in the nano-pore, this increasement was still tiny, with only a 0.54% increase in movable oil when the temperature rose by 40 K.

3.6. Different CO_2 injection amounts on the crude oil occurrence state

Fig. 10 exhibited the crude oil occurrence state with 3 CO_2 dissolution ratios in 5.92 nm pores under 380.15 K, 10 MPa. As seen from Fig. 10, more dissolved CO_2 led to an augment in CO_2 content in the adsorption layer. Besides, due to the stronger adsorption capacity of CO_2 on the rock surface, the crude oil originally adsorbed on the rock surface would be stripped off by CO_2, converting from irreducible oil to moveable oil. The main reason for this was that the adsorption capacity of CO_2 on the quartz surface was stronger than that of alkane molecules. CO_2 and alkane molecules compete for adsorption on the quartz surface. Therefore, CO_2 can strip the alkane molecules adsorbed on the quartz surface.

The crude oil density distribution shown in Fig. 11(a) can illustrate the effect of CO_2 on the oil occurrence state in nano-pores. In the absence of dissolved CO_2, the oil density of the first adsorption layer was the highest (2.25 g/cm^3). When the CO_2 solubility in crude oil was 10%, the density of the same area was 1.95 g/cm^3. Furthermore, when the CO_2 solubility reached 50%, the crude oil content in the adsorption layer decreased sharply, which was reflected in the movable oil rising to

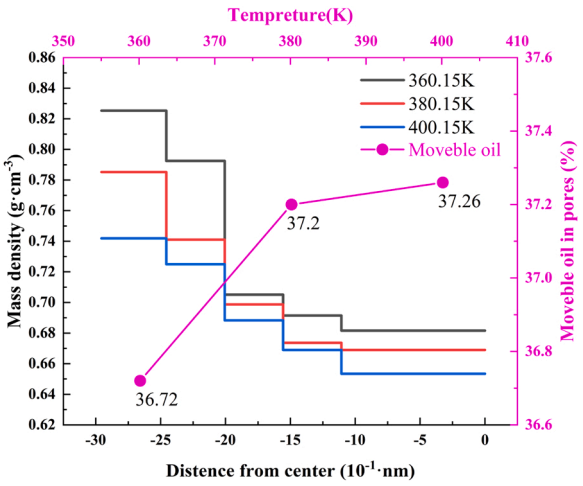

Fig. 9. Mass density discretization distribution and movable oil proportion of crude oil in 5.92 nm pore at different temperatures and a pressure of 10 MPa.

55.06% (Fig. 11(b)). In contrast, the density of bulk phase remained unaltered under different solubility conditions. This indicated that CO_2 mainly acted on the adsorbed oil but had little effect on the bulk oil.

3.7. Polar molecules on the adsorption state

To explore the effect of polar molecules on the adsorption state of crude oil in nano-pores, the acetone molecule with strong molecular polarity was selected to represent the polar molecule in crude oil, and its polarity was 5.1 [55,56]. We established two groups of MD models containing different proportions of polar molecules. Through the analysis of the simulation results, it was found that polar molecules were more easily adsorbed on the quartz surface.

Fig. 12 showed the distribution of oil molecules on the quartz surface under the different proportions of polar molecules. Compared with weaker polar alkane molecules, acetone molecules were more easily adsorbed on the solid surface in nano-pores, which depended on the properties of the solid surface and acetone. This behavior was due to the fact that the O atom in acetone and the H atom in the − OH group on the surface of quartz were more likely to form hydrogen bonds (oxygen atoms were represented Red in the liquid phase in Fig. 12).

From Fig. 13(a), the presence of polar molecules in crude oil can change the occurrence state of crude oil in nano-pores. Compared with the absence of polar molecules, the density of the first adsorption layer was significantly reduced. The main reason for this phenomenon was that the molecular weight of polar molecules selected in this paper was

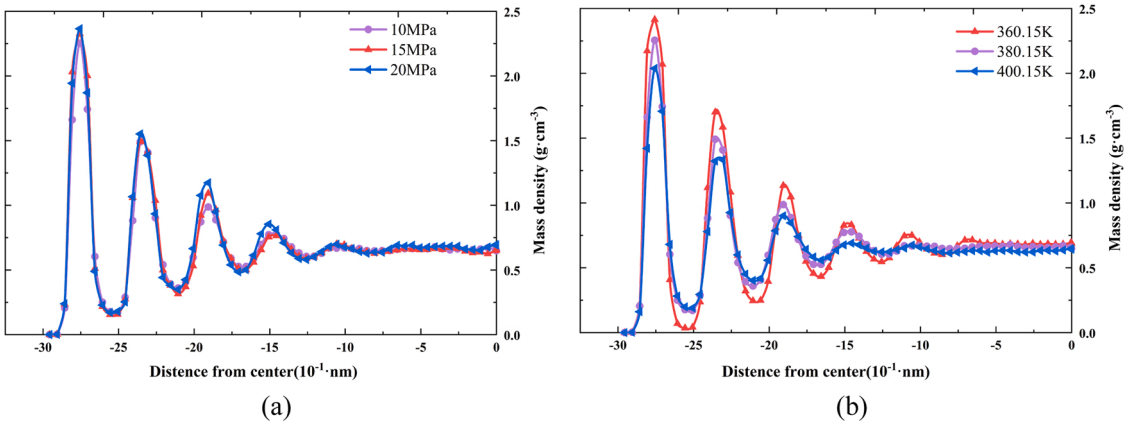

Fig. 8. Mass density discretization distribution of crude oil in 5.92 nm pore: (a) Different pressure and a temperature of 380.15 K, (b) Different temperature and pressure of 10 MPa.

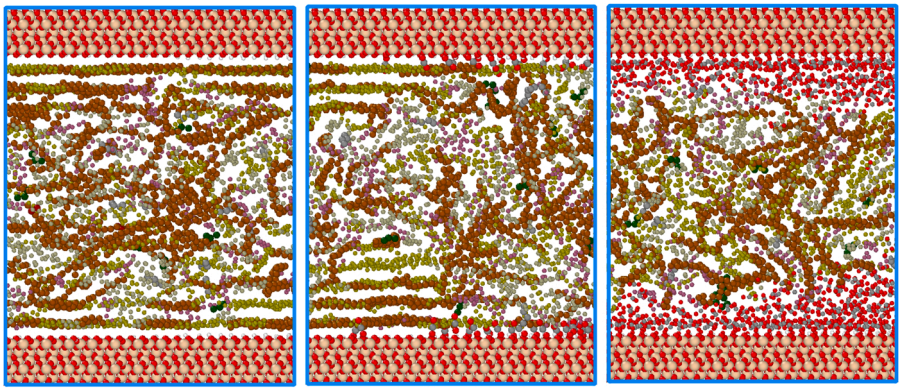

Fig. 10. Snapshot of the distribution of CO_2 and oil molecules in a 5.92 nm pore for 3 ns at a temperature of 380.15 K and a pressure of 10 MPa: (a) 0% CO_2, (b) 10% CO_2, (c) 50% CO_2.

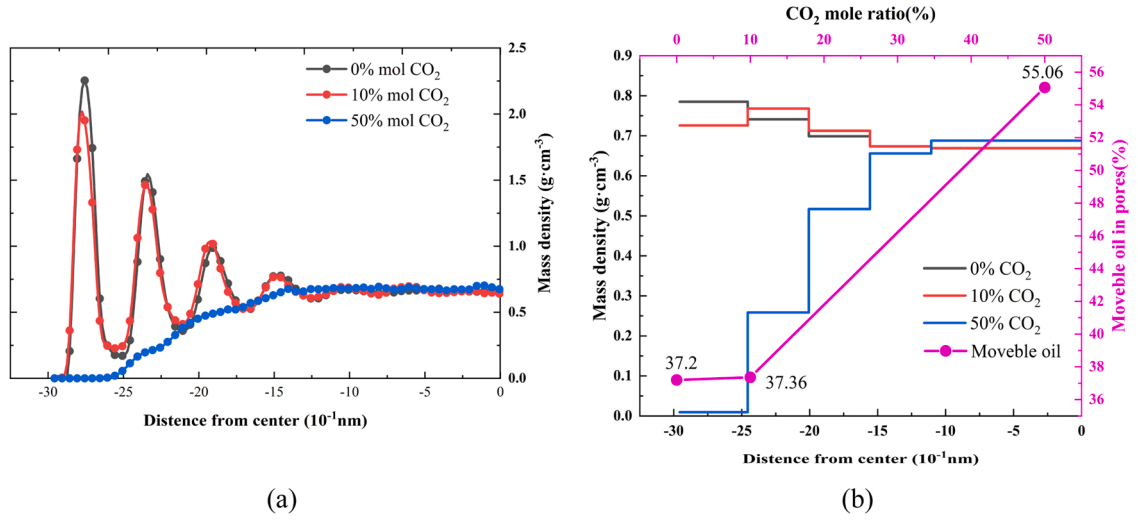

Fig. 11. Different proportions of CO2 in a 5.92 nm pore for 3 ns at a temperature of 380.15 K and a pressure of 10 MPa: (a) Density distribution, (b) Density discretization distribution, and movable oil proportion of crude oil.

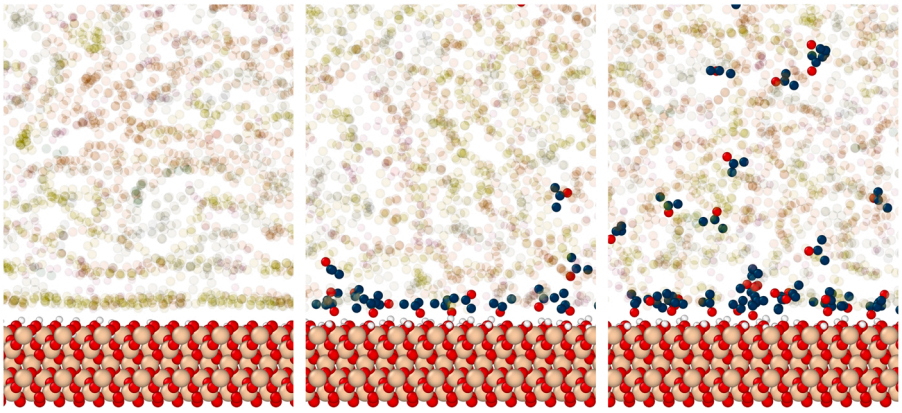

Fig. 12. Snapshots of the distribution of different proportions of polar in a 5.92 nm pore for 3 ns at a temperature of 380.15 K and a pressure of 10 MPa: (a) 0%, (b) 10%, (c) 15%.

lower than that of long-chain alkane molecules. Meanwhile, the content of polar molecules in the first adsorption layer was relatively large, resulting in a significant decrease in the density of the first adsorption layer.

From Fig. 13(b), the addition of light polar molecular acetone can increase the proportion of movable oil in crude oil, about 3%. Therefore,

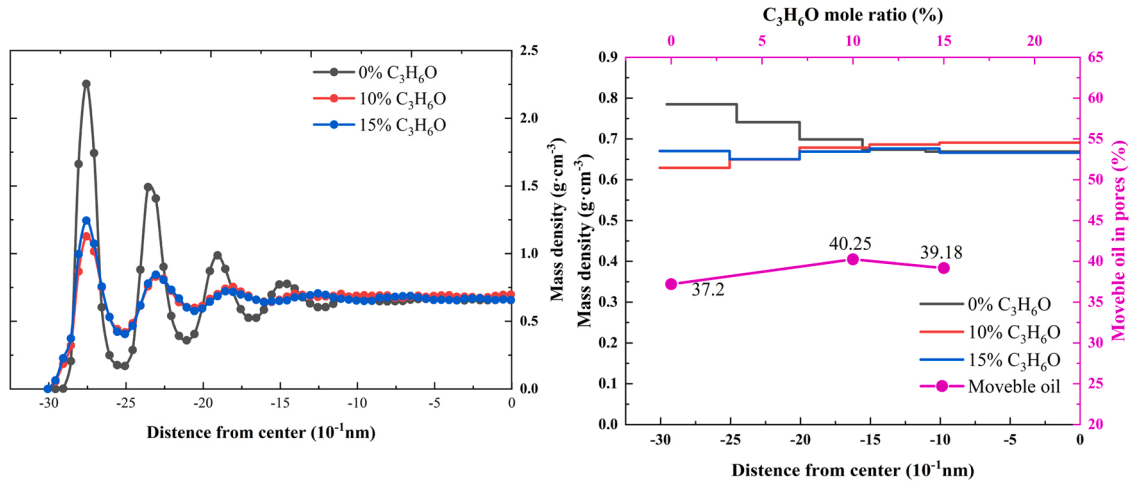

(a) (b)

Fig. 13. Density distribution in pores with different proportions of polar molecules: (a) Density distribution, (b) Density discretization distribution, and movable oil proportion of crude oil.

the polar molecules in crude oil had a certain influence on the occurrence state of crude oil. When analyzing the occurrence state of crude oil, the influence of polar molecules on the occurrence state should be considered.

4. Conclusion

In this study, the occurrence state of crude oil in nano-pores was investigated by MD method. Meanwhile, the effects of polar molecules in crude oil and CO_2 injection on the occurrence state of crude oil in nano-pores were considered. The main purpose of this study was to evaluate the distribution profiles of adsorbed and free crude oil in nano-pores. Based on the simulation results, it was observed that the adsorption state of crude oil in the quartz nano-pores was in the form of 4 adsorption layers with a thickness of 0.45 nm each. In nano-pores, the oil molecules with longer molecular chains were more likely to aggregate and adsorb on the quartz surface. In addition, the polar molecules were most easily adsorbed on water-wetted quartz surfaces. Meanwhile, the self-diffusion coefficient and potential energy of crude oil gradually increased from the vicinity of quartz wall and tended to be stable in the free layer. The average density of adsorption layers and the content of movable crude oil gradually augmented with the increasement of nanometer pore width and temperature. Oppositely, the pressure had little effect on the density distribution of crude oil in the nano-pores.

In the 5.92 nm pore, due to the stronger adsorption capacity of CO_2 on the rock surface, the crude oil originally adsorbed on the rock surface would be stripped off by CO_2, converting from the irreducible oil to the moveable oil. When the CO_2 solubility reached 50%, the crude oil content in the adsorption layer decreases sharply, which was reflected in the movable oil rising to 55.06%. It is expected that this research work will provide a theoretical basis for oil recovery enhancement practices in tight oil reservoirs.

CRediT authorship contribution statement

Yongcheng Luo: Conceptualization, Writing – original draft, Investigation, Methodology, Data curation, Formal analysis, Visualization. **Hanmin Xiao**: Resources, Funding acquisition, Supervision. **Xiangui Liu**: Project administration. **Taiyi Zheng:** Writing — review & editing, Validation. Investigation.

Declaration of Competing Interest

The authors declare that they have no known competing financial interests or personal relationships that could have appeared to influence the work reported in this paper.

Data availability

No data was used for the research described in the article.

Acknowledgments

This work was supported by the China National Petroleum Corporation (CNPC) basic advanced reserve technology (2021DJ2201).

Appendix A. Supporting information

Supplementary data associated with this article can be found in the online version at doi:10.1016/j.colsurfa.2022.130320.

References

[1] L. Yang, Z. Jin, Global shale oil development and prospects, China Petrol. Explor 24 (5) (2019) 553, https://doi.org/10.3969/j.issn.1672-7703.2019.05.002.
[2] S. Wang, Y. Liang, Q. Feng, F. Javadpour, Sticky layers affect oil transport through the nano-pores of realistic shale kerogen, Fuel 310 (2022), 122480, https://doi.org/10.1016/j.fuel.2021.122480.
[3] S. Wang, X. Yao, Q. Feng, F. Javadpour, Y. Yang, Q. Xue, X. Li, Molecular insights into carbon dioxide enhanced multi-component shale gas recovery and its sequestration in realistic kerogen, Chem. Eng. J. 425 (2021), 130292, https://doi.org/10.1016/j.cej.2021.130292.
[4] P. Zhang, S. Lu, J. Li, Characterization of pore size distributions of shale oil reservoirs: a case study from Dongying sag, Bohai Bay basin, China Mar. Petrol. Geol. 100 (2019) 297–308.
[5] P. Li, W. Sun, B. Wu, Y. Gao, K. Du, Occurrence characteristics and influential factors of movable fluids in pores with different structures of Chang 63 reservoir, Huaqing Oilfield, Ordos Basin, China Mar. Petrol. Geol. 39 (2018) 480–490.
[6] X. Wang, Y. Song, X. Guo, Q. Chang, Y. Kong, M. Zheng, Z. Qin, X. Yang, Pore-throat structure characteristics of tight reservoirs of the Middle Permian Lucaogou formation in the Jimsar Sag, Junggar Basin, northwest China, J. Pet. Sci. Eng. 208 (2022), 109245, https://doi.org/10.1016/j.petrol.2021.109245.
[7] J. Liu, L. Li, C. Zhang, Y. Jiang, R. Swennen, C. Zhao, S. Hou, Identification and quantitative evaluation of pores and throats of a tight sandstone reservoir (Upper Triassic Xujiahe Formation, Sichuan Basin, China), Mar. Pet. Geol. 140 (2022), 105663, https://doi.org/10.1016/j.marpetgeo.2022.105663.
[8] C. Li, G. Chen, X. Li, Q. Zhou, Z. Sun, The occurrence of tight oil in the Chang 8 lacustrine sandstone of the Huaqing area, Ordos Basin, China: Insights into the content of adsorbed oil and its controlling factors, J. Nat. Gas. Geosci. 7 (2022) 27–37, https://doi.org/10.1016/j.jnggs.2021.11.001.

[9] W. Wang, Y.S. Zhu, C.L. Yu, L. Zhao, D.Y. Chen, Pore size distribution in the tight sandstone reservoir of the Ordos Basin, China and their differential origin, J. Nat. Gas. Geosci. 5 (2020) 45–55.
[10] B. Bai, R. Zhu, S. Wu, W. Yang, J. Gelb, A. Gu, X. Zhang, L. Su, Multi–scale method of nano (micro)–CT study on microscopic pore structure of tight sandstone of Yanchang Formation, Ordos Basin, Petrol. Explor. Dev. 40 (3) (2013) 329–333.
[11] M. Wang, S. Zhang, F. Zhang, Y. Liu, H. Guan, J. Li, L. Shao, S. Yang, Y. She, Quantitative research on tight oil microscopic state of Chang 7 member of triassic Yanchang Formation in Ordos Basin, NW China, Petrol. Explor. Dev. 42 (6) (2015) 757–762, https://doi.org/10.1016/j.jnggs.2021.11.001.
[12] Y. Gong, S. Liu, R. Zhu, K. Liu, Z. Tang, L. Jiang, Micro-occurrence of Cretaceous tight oil in southern Songliao Basin, NE China, Petrol. Explor. Dev. 42 (3) (2015) 323–328, https://doi.org/10.1016/S1876-3804(15)30022-7.
[13] Y. Liu, X. Dong, Z. Chen, Y. Hou, Q. Luo, Y. Chen, A novel experimental investigation on the occurrence state of fluids in microscale pores of tight reservoirs, J. Pet. Sci. Eng. 196 (2021), 107656, https://doi.org/10.1016/j.petrol.2020.107656.
[14] G. Cao, Y. Bai, X. Nan, H. An, L. Wang, T. Du, D. Li, Effect of supercritical carbon dioxide adsorption on oil displacement in tight reservoir, Case Stud. Therm. Eng. 24 (2021), 100880, https://doi.org/10.1016/j.csite.2021.100880.
[15] Y. Zhang, W. Guo, Molecular insight into the tight oil movability in nano-pore throat systems, Fuel 293 (2021), 120428, https://doi.org/10.1016/j.fuel.2021.120428.
[16] M. Eslami, A.K. Ilkhchi, Y. Sharghi, N. Golsanami, Construction of synthetic capillary pressure curves from the joint use of NMR log data and conventional well logs, J. Pet. Sci. Eng. 111 (2013) 50–58.
[17] P. Zhao, Z. Wang, Z. Sun, J. Cai, L. Wang, Investigation on the pore structure and multifractal characteristics of tight oil reservoirs using NMR measurements: permian Lucaogou Formation in Jimusaer Sag, Junggar Basin, Mar. Petrol. Geol. 86 (2017) 1067–1081.
[18] E. Rosenbrand, I.L. Fabricius, Q. Fisher, C. Grattoni, Permeability in Rotliegend gas sandstones to gas and brine as predicted from NMR, mercury injection and image analysis, Mar. Petrol. Geol. 64 (2015) 189–202.
[19] M. Hekmatifar, D. Toghraie, A. Khosravi, F. Saberi, F. Soltani, R. Sabetvand, A. S. Goldanlou, The study of asphaltene desorption from the iron surface with molecular dynamics method, J. Mol. Liq. 318 (2020), 114325, https://doi.org/10.1016/j.molliq.2020.114325.
[20] Y. Yang, Z. Ma, F. Xi, X. Li, Adsorption behavior of oil-displacing surfactant at oil/water interface: Molecular simulation and experimental, J. Water Process Eng. 36 (2020), 101292, https://doi.org/10.1016/j.jwpe.2020.101292.
[21] M. Wu, Z. Zhao, G. Cai, C. Wang, G. Cheng, X. Wang, Adsorption behaviour and mechanism of benzene, toluene and m-xylene (BTX) solution onto kaolinite: Experimental and molecular dynamics simulation studies, Sep. Purif. Technol. 291 (2022), 120940, https://doi.org/10.1016/j.seppur.2022.120940.
[22] Y. Yang, J. Liu, J. Yao, J. Kou, Z. Li, T. Wu, K. Zhang, L. Zhang, H. Sun, Adsorption behaviors of shale oil in kerogen slit by molecular simulation, Chem. Eng. J. 387 (2020), 124054, https://doi.org/10.1016/j.cej.2020.124054.
[23] X. Hong, H. Yu, H. Xu, X. Wang, X. Jin, H. Wu, F. Wang, Competitive adsorption of asphaltene and n-heptane on quartz surfaces and its effect on crude oil transport through nano-pores, J. Mol. Liq. 359 (2022), 119312, https://doi.org/10.1016/j.molliq.2022.119312.
[24] H. Sui, F. Zhang, Z. Wang, D. Wang, Y. Wang, Molecular simulations of oil adsorption and transport behavior in inorganic shale, J. Mol. Liq. 305 (2020), 112745, https://doi.org/10.1016/j.molliq.2020.112745.
[25] C. Shan, W. Zhao, F. Wang, K. Zhang, Z. Feng, L. Guo, X. Ma, T. Liao, Nanoscale pore structure heterogeneity and its quantitative characterization in Chang7 lacustrine shale of the southeastern Ordos Basin, China, J. Pet. Sci. Eng. 187 (2020), 106754, https://doi.org/10.1016/j.petrol.2019.106754.
[26] H. Bu, Y. Ju, J. Tan, G. Wang, X. Li, Fractal characteristics of pores in non-marine shales from the Huainan coalfield, eastern China, J. Nat. Gas. Sci. Eng. 24 (2015) 166–177.
[27] S. Wang, Q. Feng, Javadpour, T. Xia, Z. Li, Oil adsorption in shale nano-pores and its effect on recoverable oil-in-place, Int. J. Coal Geol. 147– 148 (2015) 9–24, https://doi.org/10.1016/j.coal.2015.06.002.
[28] X. Song, J.K. Chen, A comparative study on poiseuille flow of simple fluids through cylindrical and slit-like nanochannels, Int. J. Heat. Mass Transf. 51 (2008) 1770–1779.
[29] A.A. Skelton, P. Fenter, J.D. Kubicki, D.J. Wesolowski, P.T. Cummings, Simulations of the quartz(10$\bar{1}$1)/ water interface: a comparison of classical force fields, Ab initio molecular dynamics, and X-ray reflectivity experiments, J. Phys. Chem. C. 115 (2011) 2076–2088.
[30] Y. Luan, B. Liu, P. Hao, K. Zhan, J. Liu, Oil displacement by supercritical CO_2 in a water cut dead-end pore: Molecular dynamics simulation, J. Pet. Sci. Eng. 188 (2020), 106899, https://doi.org/10.1016/j.petrol.2019.106899.
[31] F. Peng, R. Wang, Z. Guo, G. Feng, Molecular dynamics simulation to estimate minimum miscibility pressure for oil with pure and impure CO_2, J. Phys. Commun. 2 (2018), 115028, https://doi.org/10.1088/2399-6528/aaf090.
[32] C. Li, H. Pu, X. Zhong, Y. Li, J.X. Zhao, Interfacial interactions between Bakken crude oil and injected gases at reservoir temperature: A molecular dynamics simulation study, Fuel 276 (2020), 118058, https://doi.org/10.1016/j.fuel.2020.118058.
[33] J.G. Harris, K.H. Yung, Carbon dioxide's liquid–vapor coexistence curve and critical properties as predicted by a simple molecular model, J. Phys. Chem. 99 (1995) 12021–12024.
[34] M.G. Martin, J.I. Siepmann, Transferable potentials for phase equilibria. 1. unitedatom description of n-alkanes, J. Phys. Chem. B 102 (1998) 2569–2577, https://doi.org/10.1021/jp990822m.
[35] K. Polok, W. Gadomski, F. Sokolić, L. Zoranić, Molecular dynamics simulations and femtosecond optical Kerr effect spectroscopy of methanol/acetone mixtures, J. Mol. Liq. 159 159 (2011) 60–69, https://10.1016/j.molliq.2010.10.005.
[36] S.K. Nath, F.A. Escobedo, J.J.De Pablo, On the simulation of vapor-liquid equilibria for alkanes, J. Chem. Phys. 108 (1998) 9905–9911, https://doi.org/10.1063/1.476429.
[37] R.T. Cygan, J.J. Liang, A.G. Kalinichev, Molecular models of hydroxide, oxyhydroxide, and clay phases and the development of a general force field, J. Phys. Chem. B 108 (2004) 1255–1266.
[38] R. Wang, F. Peng, K. Song, G. Feng, Z. Guo, Molecular dynamics study of interfacial properties in CO_2 enhanced oil recovery, Fluid Phase Equilib. 467 (2018) 25–32, https://doi.org/10.1016/j.fluid.2018.03.022.
[39] X. Li, S. Wang, Q. Feng, Q. Xue, The miscible behaviors of C1oH22(C,H1N)/C3Hg system: Insights from molecular dynamics simulations, Fue 279 (2020), 118445, https://doi.org/10.1016/j.fuel.2020.118445.
[40] D. Do, H. Do, Adsorption of flexible n-alkane on graphitized thermal carbon black: analysis of adsorption isotherm by means of GCMC simulation, Chem. Eng. Sci. 60 (2005) 1977–1986.
[41] M. Wu, Z. Zhao, G. Cai, C. Wang, G. Cheng, X. Wang, Adsorption behaviour and mechanism of benzene, toluene and m-xylene (BTX) solution onto kaolinite: Experimental and molecular dynamics simulation studies, Sep. Purif. Technol. 291 (2022), 120940, https://doi.org/10.1016/j.seppur.2022.120940.
[42] S. Kisin, J. Bozȯvic ́Vukic ́, P.G.T. van der Varst, G. de With, C.E. Koning, Estimating the polymer metal work of adhesion from molecular dynamics simulations, Chem. Mater. 19 (2007) 903–907, https://doi.org/10.1021/cm0621702.
[43] M. Lbadaoui-Darvas, G. Garberoglio, K.S. Karadima, M.N.D.S. Cordeiro, A. Nenes, S. Takahama, Molecular simulations of interfacial systems: challenges, Appl. Future Perspect. Mol. Simul. (2021) 1–38, https://doi.org/10.1080/08927022.2021.1980215.
[44] X. Hong, H. Yu, H. Xu, X. Wang, X. Jin, H. Wu, F. Wang, Competitive adsorption of asphaltene and n-heptane on quartz surfaces and its effect on crude oil transport through nano-pores, J. Mol. Liq. 359 (2022), 119312, https://doi.org/10.1016/j.molliq.2022.119312.
[45] G. Xu, H. Wang, Molecular dynamics study of oxidative aging effect on asphalt binder properties, Fuel 188 (2017) 1–10, https://doi.org/10.1016/j.fuel.2016.10.021.
[46] X. Zhao, H. Jin, Correlation for self-diffusion coefficients of H2, CH4, CO, O2 and CO_2 in supercritical water from molecular dynamics simulation, Appl. Therm. Eng. 171 (2020), 114941, https://doi.org/10.1016/j.applthermaleng.2020.114941.
[47] H. Long, H. Lin, M. Yan, Y. Bai, X. Tong, X. Kong, S. Li, Adsorption and diffusion characteristics of CH4, CO_2, and N2 in micropores and mesopores of bituminous coal: Molecular dynamics, Fuel 292 (2021), 120268, https://doi.org/10.1016/j.fuel.2021.120268.
[48] H. Hu, L. Bao, N.V. Priezjev, K. Luo, Identifying two regimes of slip of simple fluids over smooth surfaces with weak and strong wall-fluid interaction energies, J. Chem. Phys. 146 (2017), 034701, https://doi.org/10.1063/1.4973640.
[49] R.B. Getman, Y. Bae, C.E. Wilmer, R.Q. Snurr, Review and analysis of molecular simulations of methane, hydrogen, and acetylene storage in metal-organic frameworks, Chem. Rev. 112 (2012) 703–723, https://doi.org/10.1021/cr200217c.
[50] J.H. Pacheco-Sáncheza, R. Alejoa, H. Cruz-Reyesa, F. Álvarez-Ramírez, Neural networks to fit potential energy curves from asphaltene-asphaltene interaction data, Fuel 236 (2019) 1117–1127, https://doi.org/10.1016/j.fuel.2018.09.031.
[51] C. Li, G. Chen, X. Li, Q. Zhou, Z. Sun, The occurrence of tight oil in the Chang 8 lacustrine sandstone of the Huaqing area, Ordos Basin, China: Insights into the content of adsorbed oil and its controlling factors, J. Nat. Gas. Geosci. 7 (2022) 27–37, https://doi.org/10.1016/j.jnggs.2021.11.001.
[52] Q. Xu, W. Shi, X. Xie, A.B. Busbey, L. Xu, R. Wu, K. Liu, Inversion and propagation of the Late Paleozoic Porjianghaizi fault (North Ordos Basin, China): Controls on sedimentation and gas accumulations, Mar. Pet. Geol. 91 (2018) 706–722, https://doi.org/10.1016/j.marpetgeo.2018.02.003.
[53] C.R. Clarkson, N. Solano, R.M. Bustin, A.M.M. Bustin, G.R.L. Chalmers, L. He, Y. B. Melnichenko, A.P. Radliński, T.P. Blach, Pore structure characterization of North American shale gas reservoirs using USANS/SANS, gas adsorption, and mercury intrusion, Fuel 103 (2013) 606–616.
[54] A. Harrison, R.F. Cracknell, J. Krueger-Venus, L. Sarkisov, Branched versus linear alkane adsorption in carbonaceous slit pores, Adsorption 20 (2014) 427–437.
[55] G. Åkerlöf, Dielectric constants of some organic solvent-water mixtures at various temperatures, J. Am. Chem. Soc. 54 (11) (1932) 4125–4139, https://doi.org/10.1021/ja01350a001.
[56] P. Kalhoria, A. Abbasib, M.R. Malayerib, M.M. Shirazi, Impact of crude oil components on acid sludge formation during well acidizing, J. Pet. Sci. Eng. 215 (2022), 110698, https://doi.org/10.1016/j.petrol.2022.110698.